Electrochemistry Communications 111 (2020) 106644

Contents lists available at ScienceDirect

Electrochemistry Communications

journal homepage: www.elsevier.com/locate/elecom

Ex-situ visualization of the wet domain in the microporous layer in a polymer electrolyte fuel cell by X-ray computed tomography under water vapor supply

Satoru Kato*, Satoshi Yamaguchi, Wataru Yoshimune, Yoriko Matsuoka, Akihiko Kato, Yasutaka Nagai, Takahisa Suzuki

Toyota Central R&D Labs., Inc., Nagakute City, Aichi Prefecture 480-1192, Japan

ARTICLE INFO

Keywords:
Polymer electrolyte fuel cell
Liquid water accumulation
Gas diffusion layer
X-ray computed tomography
Microporous layer

ABSTRACT

The wet domain in a microporous layer (MPL) in a polymer electrolyte fuel cell (PEFC) was visualized in order to clarify water accumulation in the MPL. The performance of PEFC is affected by accumulation of liquid water in the cathode gas diffusion layer (GDL). The liquid water hinders oxygen transport to the catalyst layer, resulting in increased mass-transport loss. Although MPLs suppress water accumulation in the GDL, this mechanism has not yet been fully clarified. The present study used synchrotron X-ray micro computed tomography (CT) to visualize water accumulation in the MPL. The experiment was conducted while supplying water vapor to the MPL side of the GDL. The MPL was visualized to be wetted heterogeneously, and liquid water movement from the MPL to the GDL substrate was visualized. These observations were supported by plotting the volume fraction of either the wet domain of the MPL or the water cluster as a function of through-plane distance.

1. Introduction

In polymer electrolyte fuel cells (PEFCs), the cathode gas diffusion layer (GDL) helps to transport oxygen and produced water. The GDL is usually composed of a substrate and a microporous layer (MPL). The substrate is commonly a carbon paper or carbon textile treated with a hydrophobic agent such as polytetrafluoroethylene (PTFE). The MPL is commonly a mixture of carbon black and PTFE. When a PEFC is operated, oxygen in the flow channels diffuses through the pores of the GDL to reach the cathode catalyst layer (CL), where the oxygen reduction reaction (ORR) takes place. Water vapor produced by ORR travels through the cathode GDL to the flow channels. The vapor condenses into liquid in the GDL when the PEFC is operated at low temperature or at high current densities. The liquid water inhibits oxygen transport, resulting in a decrease in cell potential, which is referred to as flooding. Flooding is considered to be one of the major factors that limits the performance of PEFCs [1]. Design and development of the GDL is essential in order to avoid flooding. The MPL suppresses flooding [2–5]. As Omrani and Shabani mentioned recently [6], numerous studies have tried to optimize MPLs by modifying their structural properties. For example, Gostick et al. [2] suggested that introducing large holes for water passage to the MPL is effective for the suppression of flooding. This concept was investigated and verified by Lu et al. [6], Sasabe et al. [7], Haußmann et al. [8], and Nagai et al. [9].

In order to realize the design of the GDL, the mechanisms involved in liquid water accumulation in the PEFC, such as vapor condensation and water drainage, should be clarified. Either experimental visualization of water behavior or mathematical modeling is informative. Many efforts have been made to visualize the liquid transport phenomena in PEFCs. As Bazylak summarized in their review [10], the liquid water in the gas channel, the GDL, or the membrane has been visualized using optical microscopy, neutron imaging and X-ray radiography. In addition, X-ray computed tomography (CT) has been used to visualize the water distribution in the GDL [8,9,11–14]. Mathematical modeling has also been developed in order to understand the effect of water accumulation on the performance of the PEFCs. As Liu et al. reviewed [32], approaches based on the continuum method and pore-scale simulation have been reported. Comparison between numerical results and experimentally visualized results is expected to provide detailed GDL insight into the nature of water transport through the PEFC. For example, Agaesse et al. [11] compared water invasion simulations inside the GDL based on a pore network model with X-ray tomographic images of water distributions obtained by an ex-situ water invasion experiment. The results showed good agreement between

* Corresponding author.
E-mail address: e1325@mosk.tytlabs.co.jp (S. Kato).

https://doi.org/10.1016/j.elecom.2019.106644
Received 6 November 2019; Received in revised form 18 December 2019; Accepted 18 December 2019
Available online 26 December 2019
1388-2481/ © 2019 The Author(s). Published by Elsevier B.V. This is an open access article under the CC BY license (http://creativecommons.org/licenses/BY/4.0/).

experimental and simulated microscopic water distributions. Recently, Cetinbas et al. [15] developed a dynamic model for pore-scale simulation of liquid water transport in the pores of the GDL, as measured by X-ray CT, and compared the results to the results of X-ray CT experiments reported by Zenyuk et al. [12] on the ex-situ water drainage process in the GDL. The numerical result was shown to closely match the liquid water saturation distributions obtained by the ex-situ method. The research by Agaesse et al. [11] and Cetinbas et al. [15] used the GDL, which did not have an MPL. Pore-scale simulation of water behavior in the MPL has been reported [5,15–20]. Experimentally, visualization of water behavior in the MPL is demanded.

Water accumulation in the MPL has been investigated by operando X-ray radiography and operando neutron radiography [4,6,8,21–31]. The provided results are the one-dimensional average saturation in the X-ray incidence direction. However, three-dimensional information is preferable because the water accumulates in a three-dimensionally consistent pore network in the MPL. Although operando X-ray CT experiments can provide three-dimensional information [8,9,11–14], as reported by Eller [13], the region of the MPL near the CL has been blurry due to the strong X-ray absorption by Pt loaded in the CL. This blur can be avoided for the ex-situ visualization of water injected into the GDL. However, injecting water into the pores of the MPL is difficult because the water injection requires high pressure in water. For example, assuming that the contact angle of water in pores of the MPL is 114°, which is the value of the PTFE, pressures of 119 kPa and 1188 kPa are required to inject water into the pores of diameters of 1 μm and 0.1 μm, respectively. These pressures are too high to conduct the experiment. An ex-situ experimental method to visualize water behavior in the MPL is, hence, needed.

In the present paper, a new ex-situ X-ray CT technique to explore water accumulation in MPLs is reported. In the X-ray CT experiment, water vapor diffused into the MPL side of the GDL formed liquid water in MPL. Strong X-ray absorption of Pt in the CL is avoided in the present study because only the GDL was used.

2. Experimental

Fig. 1(a) shows a custom apparatus, which was fabricated in order to conduct the experiment in the synchrotron X-ray CT beamlines. This apparatus can be used to visualize water behavior inside the MPL. The Peltier module (2) was held on the rotation stage (1). The sample stage (3) was held on the Peltier module, both of which were covered with a heat insulating material (4). Nitrogen-containing saturated water vapor at 68 °C was supplied to the MPL side of the GDL at 5 ml/min from the inlet pipe (5). The inlet pipe and the resin pipe (6) were heated to 68 °C by the heater (7). The sample was surrounded by a Kapton film (8) in order to diffuse the vapor to the space above the MPL. The area around the GDL is shown in detail in Fig. 1(b). The sample was cut to have a diameter of 5 mm and was then held by the PTFE washer (9) in order to ensure that the substrate contacts the sample stage. The surface temperature of the sample stage was 7 °C when the Peltier module was

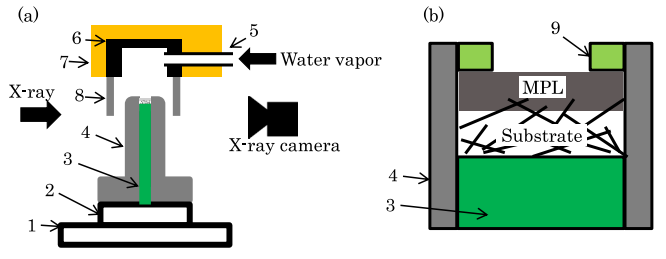

Fig. 1. (a) Schematic diagram of water vapor introduction in the experimental setup and the X-ray CT experiment, (b) Detailed description of the sample. 1: Rotation stage, 2: Peltier module, 3: Sample stage, 4: Heat insulating material, 5: Inlet pipe, 6: Resin part, 7: Heater, 8: Kapton film, 9: PTFE washer.

operated. Numerical results showed that the average temperature of the sample was 7 °C, as explained in the Supporting information. X-ray CT experiments were carried out at the TOYOTA Beamline (BL33XU) at the SPring-8 facility. The field of view, the pixel size, and the X-ray energy was 6.5 mm × 6.5 mm, 3.25 μm, and 14 keV, respectively. The sample was first scanned under the dry condition, and then water vapor was supplied. The sample was scanned at 6, 12, 18, and 24 min after vapor supply had started. GDS3260 (AvCarb Material Solutions) was used as the sample. This GDL is composed of a carbon-paper-based substrate and an MPL.

Tomographic reconstruction was carried out using a software package published by the Japan Synchrotron Radiation Research Institute (JASRI) [32]. Fiji software [33] was used for segmentation based on the procedure reported by Eller [31]. All solid phases were segmented by a global lower threshold method. The threshold was determined manually by analyzing the histogram of the dry images. In order to segment liquid water in the wet data set, difference images were obtained by subtracting the dry data set from the wet data set. With obtained data set, liquid water was segmented by global lower threshold. The threshold was determined by manually analyzing the histogram of the difference images. Visualization and evaluation of water accumulation in the GDL was performed using GeoDict® (Math2Market GmbH) software [34].

3. Results and discussion

Fig. 2(a) shows a cross-sectional image of the dry sample. In Fig. 2(a), the sample stage and substrate are shown in white. The MPL is shown in gray. Pores in the substrate and the air above the MPL are shown in black. The pore size of the MPL is observed to be on the order of sub-micrometers, as shown in Fig. S1. Note that the spatial resolution of X-ray CT in the present study is not sufficient to identify pores of MPL (See Fig. S2). Fig. 2(b) shows the same area as Fig. 2(a) and is obtained 6 min after the water vapor supply had started. The existence of liquid water can be confirmed by comparing Fig. 2(a) and (b). For example, two pores in the substrate are indicated by yellow arrows in Fig. 2(a). The brightness of the indicated area increased in Fig. 2(b). This means that water clusters exist in the indicated area. Water clusters are also observed on the MPL, as indicated by the black arrows in Fig. 2(b). Fig. 2(c) was obtained by subtracting the square region of the MPL in Fig. 2(a) from Fig. 2(b). In Fig. 2(c), the black domain, which did not change with the water vapor supply, is the dry domain. On the other hand, the white domain, in which the brightness increases with the water vapor supply, is the wet domain. As explained in the experimental section, the wet domain of the MPL and the water cluster were segmented using difference images between the dry and wet data sets.

Fig. 2(d) shows an example of a liquid water distribution in the GDL, where the dry region and wet regions of the MPL are indicated as gray and blue domains, respectively. Fig. 2(d) shows that the wet domain is unevenly distributed in the MPL. This heterogeneous wettability has not been reported in the literature and cannot be predicted based on reported results. For example, the average saturation of the MPL under the operating condition was estimated by operando X-ray radiography in the range of 0%–50% [24]. However, the three-dimensional distribution of saturation cannot be obtained by operando X-ray radiography. In addition, modeling based on the continuous method assumes homogeneous wettability for the MPL. Reported pore-scale simulation does not assume a macroscopic distribution of pores or wettability, which is considered to be a factor affecting wettability in the MPL.

Fig. 3 shows cropped three-dimensional images reconstructed from CT images obtained at 0, 6, 12, 18, and 24 min after the water vapor supply had started. Morphological change of wet domains is not observed visually from 6 min to 24 min. This means that state of wetness in the MPL reaches a steady state after 6 min. Both sides of the MPL were wetter than the inside of the MPL. This is considered to be a result of the through-plane gradient of humidity and temperature. The

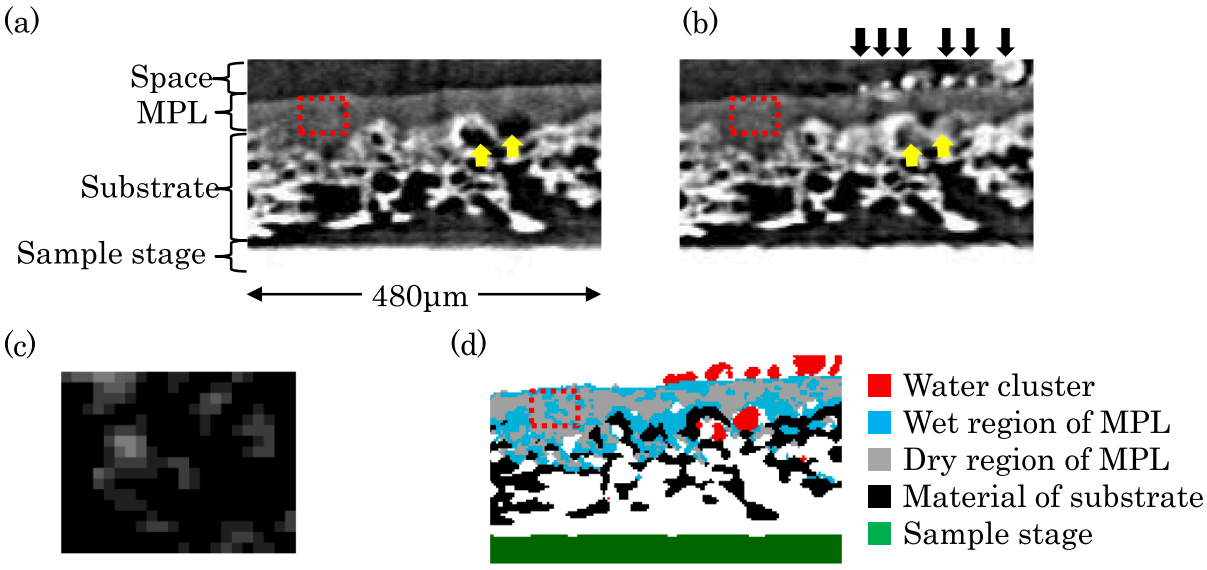

Fig. 2. (a) Cross-sectional CT image of the sample performed under the dry condition. (b) Cross-sectional CT image performed at 6 min after the water vapor supply had started, (c) Differential image obtained by subtracting the square domain of (a) from that of (b), (d) Segmented cross-sectional image.

absolute humidity in the MPL decreases from the surface side to the substrate side. This is because water vapor condenses on the outer surface of the MPL. The temperature in the MPL decreases from the surface side to the substrate side because the end side of the substrate is cooled. This allows water vapor to condense at the substrate side in the MPL. Similar through-plane saturation was obtained by operando X-ray radiography when PEFC was operated at range of 0.5 A/cm^2 and 2.0 A/cm^2 [25,26,31]. In this research, the rate of vapor supply corresponds to 1.7 A/cm^2. These similarities support the water behavior in the present study as being similar to that in the PEFC during operation.

In Fig. 3, a water cluster was observed in the pores of the substrate near the MPL at 6 min. This water cluster built up until 12 min and connected to the sample stage at 18 min. The water cluster then decreased in size until 24 min. On the other hand, the water cluster on the sample stage built up between 18 min and 24 min. This morphological change of the water cluster suggests that liquid water formed in the MPL drain to the substrate and then move to the surface on the stage.

The observation explained above will be discussed statistically in terms of the temporal change of the water distribution in the next paragraph. Before the discussion, in this paragraph, the structural properties of the GDL in the through-plane direction are explained. The upper part of Fig. 4 shows the volume fraction of the solid phase of the MPL and the substrate. The apparent gradual increase in volume fraction of the material of the MPL from 10 μm to 30 μm was caused by two factors. The X-ray beam tilted slightly away from the in-plane direction of the sample. The other factor is that the outer surface of the MPL is not smooth. Therefore, the region between 10 and 30 μm is a transition region between the space above the outer surface of the MPL and the MPL. The region between 30 and 60 μm is the MPL. The region between 60 and 120 μm is the region in which the MPL materials penetrate into the pores of the substrate. This type of region has been reported in the literature as a water accumulation region, as determined by operando radiography [23,25–30] and simulation [19]. The region between 120 and 230 μm is the substrate. The region beyond 230 μm, which is

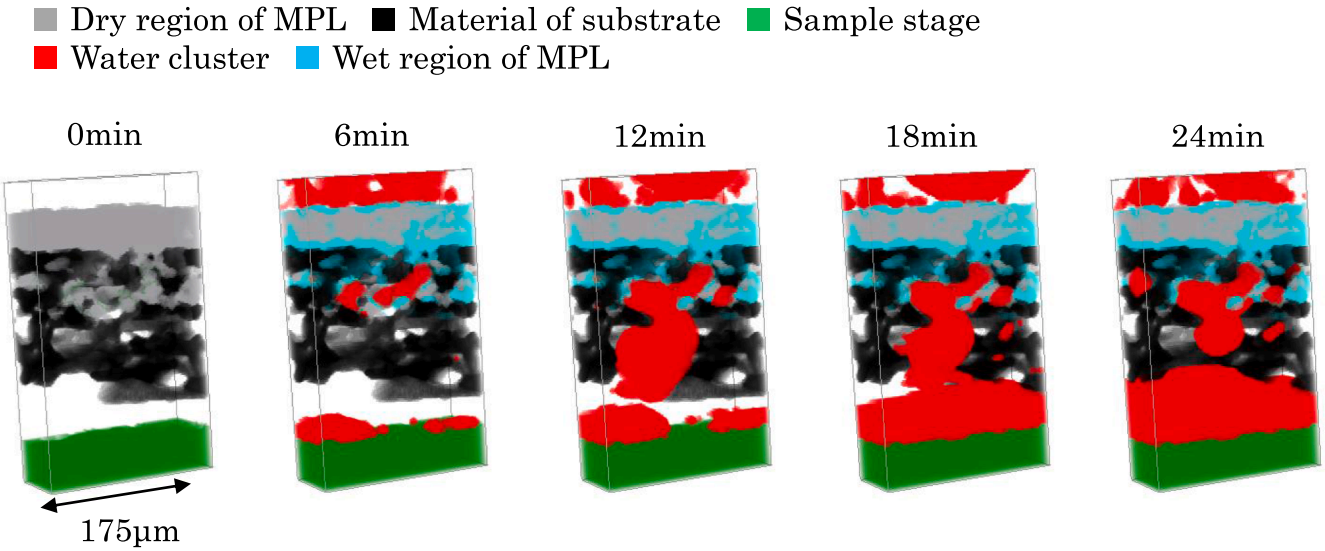

Fig. 3. Three-dimensional images reconstructed from CT images performed at 0 min, 6 min, 12 min, 18 min, and 24 min after the water vapor supply had started.

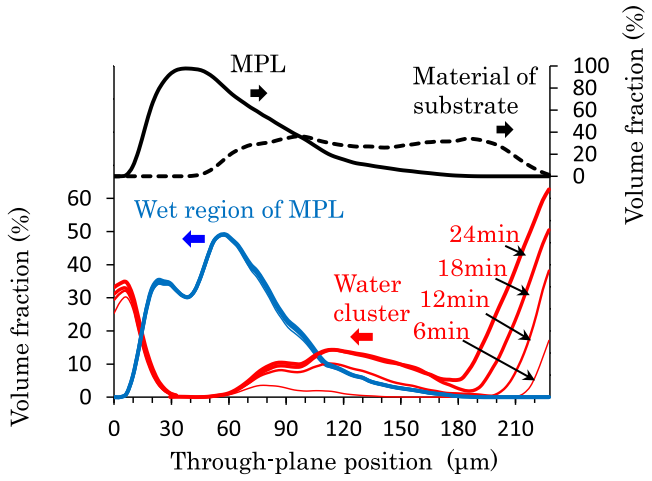

Fig. 4. Through-plane volume fraction of the MPL (black line), the material of the substrate (black dotted line), the wet region of the MPL (blue line), and the water cluster (red line). (For interpretation of the references to colour in this figure legend, the reader is referred to the web version of this article.)

omitted in Fig. 4, is the sample stage.

The lower part of Fig. 4 shows the through-plane volume fraction, which is calculated based on the total volume in the through-plane direction, of the water cluster and the wet region of the MPL. The wet region of the MPL exhibits two peaks. One peak is located at the outer surface of the MPL, and the other peak is located at the MPL penetrating region. The distribution of the wet region in the MPL did not change with time. This agrees with the observation in Fig. 3. Fig. 4 shows that either the water cluster on the MPL (10–30 μm) or the water cluster in the MPL penetration region (60–120 μm) is increased in size and/or in number with increasing supply time of water vapor. This suggests that liquid water that formed in the MPL drained to both sides of the MPL. This is supported by the fact that the volume fraction of the wet region of the MPL was in a steady state. There is no evidence that water condensation in the MPL stops under the steady state. Note that part of the water vapor condensed directly on the MPL, in the pores of the substrate, and on the sample stage. For example, in Fig. 4, the water cluster at 6 min in the position beyond 210 μm was condensed on the stage directly.

Finally, we discuss how this ex-situ visualization method is informative for understanding water accumulation in MPLs. As shown in Fig. 2(d), the MPL held water heterogeneously. This is considered as having resulted from 1) the distribution of the pore size and connectivity and 2) the distribution of the hydrophobicity. For example, the reported numerical results suggest that the water cluster is stabilized in larger pores [20,35]. The distribution of the hydrophobicity may be related to the heterogeneous distribution of the PTFE in the MPL, which was visualized by X-ray nano CT [36]. Fig. 4 suggests that liquid water formed in the MPL was drained to the outer surface of the MPL. This may correspond to water accumulation at the interface between the MPL and the CL. Water accumulation at the interface was observed by operando X-ray radiography [21,22]. The advantage of the ex-situ method is that water accumulation can be investigated in three directions. For example, the effects of surface structure (ex. roughness and cracks) on water accumulation can be investigated by the method described in the present study. In addition, Fig. 4 suggests that liquid water formed in the substrate side of the MPL was drained to the pores of the substrate. This is expected to be helpful to investigate the effect of large pores on water accumulation in the GDL. For example, Nagai et al. suggested that the presence of large pores in the MPL facilitates the merging of many liquid water pathways generated in the catalyst layer and so forms stable primary pathways that readily connect water clusters in the substrate [9]. This suggestion is expected to be verified by the ex-situ method. As discussed above, the ex-situ method is expected to contribute to clarification of the water behavior in the MPL and to the design of the MPL.

4. Conclusion

Water vapor condensation in the GDL was investigated by ex-situ X-ray CT. The experiment was conducted while either cooling the substrate side of the GDL with a Peltier module or supplying water vapor to the MPL side of the GDL. Water vapor condensation demonstrated that the MPL was wetted heterogeneously. The liquid water movement from the MPL to the sample stage throughout the substrate was also demonstrated. The liquid water distribution in the through-plane direction indicated that liquid water formed in the MPL drained to both sides of the MPL. The water distribution reached a steady state within the first 6 min after water vapor supply had started. The combination of ex-situ measurement in this research and the operando visualization experiment is expected to contribute to the comprehensive understanding of water accumulation in the MPL.

CRediT authorship contribution statement

Satoru Kato: Conceptualization, Methodology, Formal analysis, Investigation, Writing - original draft, Visualization. **Satoshi Yamaguchi:** Methodology, Validation, Investigation, Data curation. **Wataru Yoshimune:** Investigation, Writing - review & editing. **Yoriko Matsuoka:** Investigation. **Akihiko Kato:** Investigation. **Yasutaka Nagai:** Investigation, Supervision. **Takahisa Suzuki:** Writing - review & editing, Project administration.

Declaration of Competing Interest

The authors declare that they have no known competing financial interests or personal relationships that could have appeared to influence the work reported in this paper.

Acknowledgements

The synchrotron radiation experiments were performed at the BL33XU of SPring-8 with the approval of JASRI (proposal Nos. 2017A7032, 2017B7032, 2018A7032, 2018B7032, and 2019A7032).

Appendix A. Supplementary data

Supplementary data to this article can be found online at https://doi.org/10.1016/j.elecom.2019.106644.

References

[1] H. Wu, A review of recent development: transport and performance modeling of PEM fuel cells, Appl. Energy 165 (2016) 81–106.
[2] J.T. Gostick, M.A. Ioannidis, M.W. Fowler, M.D. Pritzker, On the role of the microporous layer in PEMFC operation, Electrochem. Commun. 11 (2009) 576–579.
[3] J.P. Owejan, J.E. Owejan, W. Gu, T.A. Trabold, T.W. Tighe, M.F. Mathias, Water transport mechanisms in PEMFC gas diffusion layers, J. Electrochem. Soc. 157 (2010) B1456–B1464.
[4] P. Oberholzer, P. Boillat, R. Siegrist, A. Kästner, E.H. Lehmann, G.G. Scherer, A. Wokaun, Simultaneous neutron imaging of six operating PEFCs: experimental set-up and study of the MPL effect, Electrochem. Commun. 20 (2012) 67–70.
[5] D. Zhang, Q. Cai, S. Gu, Three-dimensional lattice-Boltzmann model for liquid water transport and oxygen diffusion in cathode of polymer electrolyte membrane fuel cell with electrochemical reaction, Electrochim. Acta 262 (2018) 282–296.
[6] Z. Lu, J. Waldecker, X. Xie, M.C. Lai, D.S. Hussey, D.L. Jacobson, Investigation of water transport in perforated gas diffusion layer by neutron radiography, ECS Trans. 58 (2013) 315–324.
[7] T. Sasabe, P. Deevanhxay, S. Tsushima, S. Hirai, Soft X-ray visualization of the liquid water transport within the cracks of micro porous layer in PEMFC, Electrochem. Commun. 13 (2011) 638–641.
[8] J. Haußmann, H. Markötter, R. Alink, A. Bauder, K. Dittmann, I. Manke, J. Scholta, Synchrotron radiography and tomography of water transport in perforated gas diffusion media, J. Power Sources 239 (2013) 611–622.

[9] Y. Nagai, J. Eller, T. Hatanaka, S. Yamaguchi, S. Kato, A. Kato, F. Marone, H. Xu, F.N. Büchi, Improving water management in fuel cells through microporous layer modifications: fast operando tomographic imaging of liquid water, J. Power Sources 435 (2019) 226809.
[10] A. Bazylak, Liquid water visualization in PEM fuel cells: a review, Int. J. Hydrogen Energy 34 (2009) 3845–3857.
[11] T. Agaesse, A. Lamibrac, F.N. Büchi, J. Pauchet, M. Prat, Validation of pore network simulations of ex-situ water distributions in a gas diffusion layer of proton exchange membrane fuel cells with X-ray tomographic images, J. Power Sources 331 (2016) 462–474.
[12] I.V. Zenyuk, D.Y. Parkinson, G. Hwang, A.Z. Weber, Probing water distribution in compressed fuel-cell gas-diffusion layers using X-ray computed tomography, Electrochem. Commun. 53 (2015) 24–28.
[13] J. Eller, J. Roth, F. Marone, M. Stampanoni, F.N. Büchi, Operando properties of gas diffusion layers: saturation and liquid permeability, J. Electrochem. Soc. 164 (2) (2017) F115–F126.
[14] J. Eller, T. Rosén, F. Marone, M. Stampanoni, A. Wokaun, F.N. Büchi, Progress in in-situ X-ray tomographic microscopy of liquid water in gas diffusion layers of PEFC, J. Electrochem. Soc. 158 (2011) B963–B970.
[15] F.C. Cetinbas, R.K. Ahluwalia, A.D. Shum, I.V. Zenyuk, Direct simulations of pore-scale water transport through diffusion media, J. Electrochem. Soc. 166 (2019) F3001–F3008.
[16] K.N. Kim, J.H. Kang, S.G. Le, J.H. Nam, C.-J. Kim, Lattice Boltzmann simulation of liquid water transport in microporous and gas diffusion layers of polymer electrolyte membrane fuel cells, J. Power Sources 278 (2015) 703–717.
[17] V.P. Schulz, E.A. Wargo, E.C. Kumbur, Pore-morphology-based simulation of drainage in porous media featuring a locally variable contact angle, Transp Porous Med 107 (2015) 13–25.
[18] C. Qin, S.M. Hassanizadeh, L.M.V. Oosterhout, Pore-network modeling of water and vapor transport in the micro porous layer and gas diffusion layer of a polymer electrolyte fuel cell, Computation 4 (2016) 21.
[19] A.K.C. Wong, R. Banerjee, A. Bazylak, Tuning MPL intrusion to increase oxygen transport in dry and partially saturated polymer electrolyte membrane fuel cell gas diffusion layers, J. Electrochem. Soc. 166 (2019) F3009–F3019.
[20] A. Pournemat, F. Wilhelm, J. Haußmann, S. Vierrath, S. Thiele, J. Scholta, A steady-state monte carlo study on the effect of structural and operating parameters on liquid water distribution within the microporous layers and the catalyst layers of PEM fuel cells, J. Electrochem. Soc. 165 (2018) F1092–F1097.
[21] H. Naito, T. Jao, T. Yoshida, T. Sasabe, K. Kawamura, S. Hirai, Visualization of liquid water distribution at interfaces of PEFC by using parallel-beam soft X-ray radiography, ECS Trans. 80 (2017) 425–431.
[22] T. Swamy, E.C. Kumbur, M.M. Mench, Characterization of interfacial structure in PEFCs: water storage and contact resistance model, J. Electrochem. Soc. 157 (2010) B77–B85.
[23] J. Lee, H. Liu, M.G. George, R. Banerjee, N. Ge, S. Chevalier, T. Kotaka, Y. Tabuchi, A. Bazylak, Microporous layer to carbon fibre substrate interface impact on polymer electrolyte membrane fuel cell performance, J. Power Sources 422 (2019) 113–121.
[24] J. Lee, S. Chevalier, R. Banerjee, P. Antonacci, N. Ge, R. Yip, T. Kotaka, Y. Tabuchi, A. Bazylak, Investigating the effects of gas diffusion layer substrate thickness on polymer electrolyte membrane fuel cell performance via synchrotron X-ray radiography, Electrochim. Acta 236 (2017) 161–170.
[25] P. Antonacci, S. Chevalier, J. Lee, N. Ge, J. Hinebaugh, R. Yip, Y. Tabuchi, T. Kotaka, A. Bazylak, Balancing mass transport resistance and membrane resistance when tailoring microporous layer thickness for polymer electrolyte membrane fuel cells operating at high current densities, Electrochim. Acta 188 (2016) 888–897.
[26] J. Lee, R. Yip, P. Antonacci, N. Ge, T. Kotaka, Y. Tabuchi, Synchrotron investigation of microporous layer thickness on liquid water distribution in a PEM fuel cell, J. Electrochem. Soc. 162 (2015) F669–F676.
[27] T. Kotaka, Y. Tabuchi, U. Pasaogullari, C. Wang, Impact of interfacial water transport in PEMFCs on cell performance, Electrochim. Acta 146 (2014) 618–629.
[28] C. Hartnig, I. Manke, R. Kuhn, N. Kardjilov, J. Banhart, W. Lehnert, Cross-sectional insight in the water evolution and transport in polymer electrolyte fuel cells, Appl. Phys. Lett. 92 (2008) 134106.
[29] P. Deevanhxay, T. Sasabe, S. Tsushima, S. Hirai, Effect of liquid water distribution in gas diffusion media with and without microporous layer on PEM fuel cell performance, Electrochem. Commun. 34 (2013) 239–241.
[30] J.S. Preston, R.S. Fu, U. Pasaogullari, D.S. Hussey, D.L. Jacobson, Consideration of the role of micro-porous layer on liquid water distribution in polymer electrolyte fuel cells, J. Electrochem. Soc. 158 (2011) B239–B246.
[31] R. Banerjee, N. Ge, J. Lee, M.G. George, S. Chevalier, H. Liu, P. Shrestha, D. Muirhead, A. Bazylak, Transient liquid water distributions in polymer electrolyte membrane fuel cell gas diffusion layers observed through in-operando synchrotron X-ray radiography, J. Electrochem. Soc. 164 (2017) F154–F162.
[32] K. Uesugi, Computed Tomography in SPring-8 (SP-μCT), SPring-8 Web Site, http://www-bl20.spring8.or.jp/xct/.
[33] C.A. Schneider, W.S. Rasband, K.W. Eliceiri, NIH image to ImageJ: 25 years of image analysis, Nat. Methods 9 (2012) 671–675.
[34] I.T.W.M. Fraunhofer, Department Flow and Material Simulation, GeoDict, Kaiserslautern, Germany, https://www.itwm.fraunhofer.de/en/departments/sms/products-services/geodict-digital-material-laboratory.html.
[35] T. Hutzenlaub, J. Becker, R. Zengerle, S. Thiele, Modelling the water distribution within a hydrophilic and hydrophobic 3D reconstructed cathode catalyst layer of a proton exchange membrane fuel cell, J. Power Sources 227 (2013) 260–266.
[36] M. Andisheh-Tadbir, F.P. Orfino, E. Kjeang, Three-dimensional phase segregation of micro-porous layers for fuel cells by nano-scale X-ray computed tomography, J. Power Sources 310 (2016) 61–69.